Thermogravimetric characteristics and kinetics of herb residues catalyzed by potassium carbonate

Hongyu Zhu, Lin Lang, Gang Fang, Dingying Na, Xiuli Yin, Xi Yu, Chuangzhi Wu, Anthony V. Bridgwater

PII: S0165-2370(21)00156-X

DOI: https://doi.org/10.1016/j.jaap.2021.105170

Reference: JAAP 105170

To appear in: *Journal of Analytical and Applied Pyrolysis*

Received Date: 14 March 2021

Revised Date: 16 April 2021

Accepted Date: 18 April 2021

Please cite this article as: Zhu H, Lang L, Fang G, Na D, Yin X, Yu X, Wu C, Bridgwater AV, Thermogravimetric characteristics and kinetics of herb residues catalyzed by potassium carbonate, *Journal of Analytical and Applied Pyrolysis* (2021), doi: https://doi.org/10.1016/j.jaap.2021.105170

Thermogravimetric characteristics and kinetics of herb residues catalyzed by potassium carbonate

Hongyu Zhu[1,2], Lin Lang [2*], Gang Fang[2,3], Dingying Na[2], Xiuli Yin[2], Xi Yu[1*], Chuangzhi Wu[2,3,4], Anthony V. Bridgwater[1]

1.Energy & Bioproducts Research Institute (EBRI), College of Engineering and Physical Sciences, Aston University, Aston Triangle, Birmingham B4 7ET, United Kingdom.

2. CAS Key Laboratory of Renewable Energy, Guangzhou Institute of Energy Conversion, Chinese Academy of Sciences, Guangzhou 510640, China.

3. School of Engineering Science, University of Science and Technology of China, Hefei 230026, China.

4. University of Chinese Academy of Sciences, Beijing 100049, People's Republic of China

Corresponding authors: Lin Lang (langlin@ms.giec.ac.cn) and Xi Yu (x.yu3@aston.ac.uk)

Highlights

- Pyrolysis temperature of decocted CHR is higher than conventional lignocellulosic biomass
- Catalytic activity is most significant in the main devolatilization stage at 425-700K
- K_2CO_3 dramatically promotes the catalytic pyrolysis of hemicellulose and cellulose
- Pyrolysis kinetics can be described by Starink method and single-step D_n-Jader model
- Values of *n* and *A* tend to change measurably with heating rates for CHR loading K_2CO_3

Abstract

Thermal conversion technology of Chinese herb residues (CHR) becomes one of the most promising technologies in the large-scale clean utilization of herb residues due to its short process and high efficiency. In this study, non-isothermal thermogravimetric analysis of CHR samples without and with K_2CO_3 (5%K- 9%K) was implemented at 300-1125 K and the heating rates of 10-40 K/min. A model-free Starink method was applied to evaluate the thermal decomposition behavior and apparent activation energy (E_α) values. The estimated average activation energy decreases from 206.3kJ/mol of raw CHR to 143.8-160.6 kJ/mol of CHR with K_2CO_3. K_2CO_3 catalysts significantly promote the catalytic pyrolysis reaction of the hemicellulose and cellulose of CHR samples at the main devolatilization stage from 425K to 700K with over 82.02% mass loss. The pyrolysis temperature of the raw CHR is higher than traditional lignocellulosic biomass without decoction. By using the generalized master-plots method, it was found that the CHR pyrolysis could be described by a modified Dn-Jader model, but values of *n* and *A* tend to change measurably with heating rates for the CHR samples with catalysts due to the remarkably catalytic effect of K_2CO_3.

Keywords: Herb residues; Catalytic pyrolysis; Kinetic analysis; Thermogravimetry; Potassium carbonate

Nomenclature

Abbreviations

CHR	Chinese herb residues
CMM	Chinese medicinal materials

Roman symbols

A	Pre-exponential factor in Arrhenius expression
D_n	Kinetic model
D	Pyrolysis characteristic index
E_α	Apparent activation energy
E_0	Average activation energy
n	Coefficient of kinetic model
R	Universal gas constant
T	Temperature
t	Time
x	thickness of the reaction zone
α	Conversion rates
β	Heating rates
$f(\alpha)$	Differential mechanism function
$G(\alpha)$	Integrated mechanism function
$P(u)$	Temperature integral

1. Introduction

China is the world's most imperative manufacturer and consumer of Chinese medicinal materials (CMM)，and the annual CMM discharge is about 5.0 million tons [1]. Due to the rapid development of the Chinese medicine industry, especially for the widespread use of traditional Chinese medicine in the effective control of COVID-19 infection [2], there are annually more than 15 million tons of "herb residue" with high water content after the extraction of medical active components from CMM herbs, and it has been maintained an annual rate of around 15%. However, the herb residue is easy to decay and is potentially harmful to the environment, based

on the traditional treatment processes such as composting and landfilling. How to reuse and recycle this special solid waste is a very urgent significant job, yet a devil of a tricky problem.

Chinese herb residues (CHR) are also a kind of biomass waste, which could be employed as a renewable energy source via biomass thermal conversion technology, which is one of the most promising technologies in the large-scale clean utilization of herb residues due to its short process and high efficiency [3,4]. As the base unit of thermochemical conversion, pyrolysis is the initial or accompanying reaction of gasification, liquefaction and carbonization; therefore, the study of pyrolysis characteristics and kinetic analysis of herb residence will be beneficial to the development of new and efficient thermochemical conversion technologies, as well as optimizing the design of proper reactors [5].

Compared with other biomass such as stalks, straws, and wood residues, chemical compositions of the decocted CHR were significantly different, which suggested special pyrolytic behaviors [6]. This investigative topic remains a puzzled issue. Recently, several reports had proved that the catalytic pyrolysis of CHR was a solution with great application prospects, such as, the preparation of hydrogen-rich gas and the effective removal of CO_2 using Ni/CaO catalysts [7,8], upgrading the quality of bio-oil by ZSM-5 catalysts [9,10], and in-situ CO_2 capture promoted by CaO catalysts [11,12]. However, the catalytic properties of potassium salts were rarely reported for the CHR materials, which has attracted much attention in recent years due to the exceptional catalytic effect of potassium on the on the pyrolysis and gasification for the traditional biomass [13,14].

Therefore, this work is will focus on the following two aspects. First of all, the effect of potassium carbonate on CHR pyrolysis properties was investigated by impregnating different amounts of K_2CO_3, using a thermogravimetric analyzer and a Model-free kinetic analysis method. The advantage of model-free method is to calculate the apparent activation energy values without the assumption of differential mechanism functions of the reaction. Numerous reports had showed that the calculation results obtained from the Model-free method give a better description of the pyrolysis process of biomass [15,16], especially for the Starink method [14,17]. On the other hand, the Model-free method only offers very limited kinetic information, except the activation energy and pre-exponential factor. For more comprehensive kinetic analysis, the determination of significant mechanism function is very important. Although various reaction schemes have been developed to describe the mechanism functions [5,18-21], they always appear to be inconvenient when using these complex reaction models, which involves a lot of unknown kinetic parameters that cannot be simply obtained by traditional model-free methods. In this paper, the reaction mechanism and pre-exponential factor were analyzed by using the generalized master-plots method, and the model results using the optimized parameters were compared with the experimental data at various heating rates. It is anticipated that the current work should be instructive for further kinetic analysis of catalytic pyrolysis of herb residues.

2. Materials and methods

2.1 Materials

The CHR powder (60 mesh) was selected in the experiment and purchased from Guangdong Jiuqi Ecological Environment Technology Co., Ltd. The raw material is a kind of herbaceous CHR waste during the production of proprietary Chinese medicine manufactured by Guangdong Jiuhe Pharmaceutical Co., Ltd. Table 1 shows the proximate and ultimate analyses results of herb residue. The chemical reagents were analytical grade and purchased from Aladdin (Shanghai) Chemical Reagent CO., Ltd., the experimental gases were purchased from Guangzhou Yuejia Gas Co., Ltd., including high-purity nitrogen (purity ≥99.999%), high-purity argon (99.999%) and other standard gases.

Table 1: Proximate and ultimate analyses of herb

Samples	Proximate analyses (wt%)			Ultimate analyses (wt%)			
	A_d	V_d	FC_d	C_{daf}	H_{daf}	N_{daf}	O^*_{daf}
herb residue	3.37	80.87	15.76	46.91	6.06	0.79	42.88

*****(by difference.)

In this work, the catalyst of potassium carbonate (K_2CO_3, 99.0 wt%) was loaded on the CHR powder by impregnation method as follows: firstly, K_2CO_3 and deionized water were mixed to make a catalyst solution; and then slowly dripped into the dry herb residue and well stirred; finally, the sample was dried in an air-circulating oven at 378K for over 12.0 h, after aging at 273K for about 12.0 h in a refrigerator. The dried sample was crushed in an agate mortar, and the fractions of particle size <60 mesh was selected. According to the mass fraction of potassium, as shown in Table 2, the samples loading K_2CO_3 are marked as Herb-5%K, Herb-7%K and Herb-9%K, respectively. The raw CHR material was treated with a similar method, just replaced the catalyst solution with the same quality of deionized water and marked the dried CHR sample as Herb.

Table 2: The main inorganic elements in the herb samples, determined by ICP-OES*

Samples	K	Ca	Mg	Fe	Si
Herb	0.36	0.96	0.13	0.11	0.06
Herb-5%K	4.89	0.96	0.12	0.12	0.06
Herb-7%K	6.59	0.85	0.11	0.12	0.08
Herb-9%K	8.90	0.84	0.10	0.11	0.11

* wt.% by weight, Dry basis

2.2 Thermogravimetric analysis

Thermogravimetric analysis of each sample was implemented by TA SDT650 rapid temperature-increasing

thermogravimetric analyzer manufactured by TA Instruments in U.S.A. About 5.00 mg of dry-based sample was placed in an Al_2O_3 crucible. The carrier gas is high-purity nitrogen with the gas flow rate of 100 ml/min. The heating interval is 300-1125 K, with different programmed heating rates (β_1=10 K/min, β_2=20 K/min, β_3=30 K/min, β_4=40 K/min, and β_5=15 K/min).

To illustrate the weight loss of the CHR in different pyrolysis process stages. The mass loss ratio is defined in Eq. (1), which is the ratio of the mass loss at different stage to the total mass loss.

$$\Delta Mass_i = \frac{Mass\ loss\ at\ stage\ i}{Total\ mass\ loss} \times 100\% \quad (1)$$

Where i = 1, 2, 3, represents one of three pyrolysis stages including dehydration, devolatilization and carbonization respectively. The detailed results will be discussed in Section 3.2.

2.3 Kinetic parameters study

The Arrhenius dynamics formula applied in the solid-state biomass thermal decomposition kinetics could be described as:

$$\frac{d\alpha}{dt} = A \exp\left(-\frac{E_\alpha}{RT}\right) f(\alpha) \quad (2)$$

$$\alpha = \frac{m_0 - m_t}{m_0 - m_\infty} \quad (3)$$

Where t is the reaction time (s), α is the conversion rate (%), m_0, m_t, m_∞ represent the initial sample mass, the sample mass at the time t, and the final sample mass, respectively. A is the pre-exponential factor of Arrhenius (s^{-1}), E_α is the apparent activation energy (kJ/mol), T is the Kelvin temperature (K), and R is the universal gas constant, valued 8.314×10^{-3} kJ/(mol·K), $f(\alpha)$ is the differential mechanism function, depending on the reaction model (Table 3).

For the non-isothermal kinetics (β = dT/dt, K·s^{-1}), introducing a constant heating rate β into the Eq. (2):

$$\frac{d\alpha}{dT} = \frac{A}{\beta} \exp\left(-\frac{E_\alpha}{RT}\right) f(\alpha) \quad (4)$$

The integrated mechanism function ($G(\alpha)$) can be obtained from the integration of Eq. (4):

$$G(\alpha) = \frac{A}{\beta} \int_0^T \exp(-\frac{E_\alpha}{RT})\, \mathrm{d}T \quad (5)$$

$$G(\alpha) = \frac{AE_\alpha}{\beta R} P(u) \quad (6)$$

In Eq. (6), the P(u) is named as temperature integral, where $u = E_0/(RT)$, E_0 is the average activation energy. Although there is no analytical solution in common sense, a number of approximate methods have been

developed to solve the *P*(u) [22]. Starink [17] summarized the advantages and disadvantages of Kissinger, Ozawa and Boswell equations, and proposed a more accurate non-isothermal TG analysis method to determine the activation energy of pyrolytic reactions with multi heating rates and model-free kinetics.

The Starink's approximation [17,23] of the temperature integral equation in the range of $20 \leq u \leq 60$, is given as:

$$P(u) = \frac{\exp(-1.0008u - 0.312)}{u^{1.92}} \tag{7}$$

As a result, the apparent activation energy could be calculated by the Starink equation given by [18]:

$$ln\frac{\beta}{T^{1.92}} = -1.0008\frac{E_\alpha}{RT} + ln\frac{A\,R^{0.92}}{G(\alpha)\,E_\alpha^{0.92}} - 0.312 \tag{8}$$

where the linear relationship exists between $1/T$ and $ln(\beta/T^{1.92})$, and the activation energy E_α at the conversion rate α can be obtained from the slope of the curve at different heating rates, by plotting the linear fitting model of $1/T$ against $ln(\beta/T^{1.92})$ for the whole conversion process. The average activation energy (E_0) is the arithmetical average value of E_α in the range of $0.10 \leq \alpha \leq 0.74$.

Based on the model-free kinetic results, the generalized master-plot method was used for the determination of the reaction model and its mechanism function by comparing experimental data with the theoretical master curves. Master-plot method is based on the integral mechanism function ($G(\alpha)$) shown in Table 3. From the integral kinetic equation, Eq.(6)&(7), at reference point $\alpha = 0.5$, the following equation is obtained [24]:

$$\frac{G(\alpha)}{G(0.5)} = \frac{P(u)}{P(u_{0.5})} \tag{9}$$

The suitable pyrolysis reaction mechanism is the master-plot curve which best represents the experimental data, once $G(\alpha)$ has been determined, the pre-exponential factors (A_α) can be estimated from the Eq. (8).

Table 3: Ten different widely used mechanism functions of solid-state reaction models [25].

Mechanism Models	**Symbol**	***f*(α)**	***G*(α)**
Contracting area	R2	$(1-\alpha)^{1/2}$	$2[1-(1-\alpha)^{1/2}]$
Contracting volume	R3	$(1-\alpha)^{2/3}$	$3[1-(1-\alpha)^{1/3}]$
Nucleation (Johnson-Mehl-Avrami)	Am	$m(1-\alpha)\,[-\ln(1-\alpha)]^{1-1/m}$	$[-\ln(1-\alpha)]^{-1/m}$
1-D diffusion	D1	$1/(2\alpha)$	α^2
2-D diffusion	D2	$[-\ln(1-\alpha)]^{-1}$	$\alpha+(1-\alpha)\ln(1-\alpha)$
3-D diffusion-Jander	D3	$[(3/2)(1-\alpha)^{1/3}]/[1-(1-\alpha)^{1/3}]$	$[1-(1-\alpha)^{1/3}]^2$
Ginstling-Brounshtein	D4	$(3/2)/[(1-\alpha)^{1/3}-1]$	$(1-2\alpha/3)-(1-\alpha)^{2/3}$
First-order reaction	L1	$1-\alpha$	$-\ln(1-\alpha)$
Second-order reaction	L2	$(1-\alpha)^2$	$(1-\alpha)^{-1}-1$
Third-order reaction	L3	$(1-\alpha)^3$	$[(1-\alpha)^{-2}-1]/2$

3. Results and discussion

3.1 Sample characterization

Raw CHR contains low nitrogen (0.79 wt%) and high amount of volatiles (80.87 wt%) shown in Table 1, which indicates that the CHR material could be a desirable feedstock for thermochemical conversion [26]. Moreover, the ash content of raw CHR sample (3.37 wt%) is lower than the conventional biomass materials [5], such as wheat straw (6.01 wt%) and rape straw (5.63 wt%), which may be due to the fact that most of the soluble inorganic minerals will be removed from CHR during the decocting process, especially the potassium.

In this study, the K_2CO_3 catalyst was loaded on the raw CHR powder by impregnation method with different content, as shown in Table 2, in order to investigate the catalytic properties of potassium salts for the CHR materials. The K_2CO_3 catalyst is highly stable and kinetically favorable. The stability of K_2CO_3 catalyst is shown in Figure S1.

3.2 TG analysis of CHR samples with K_2CO_3 catalysts

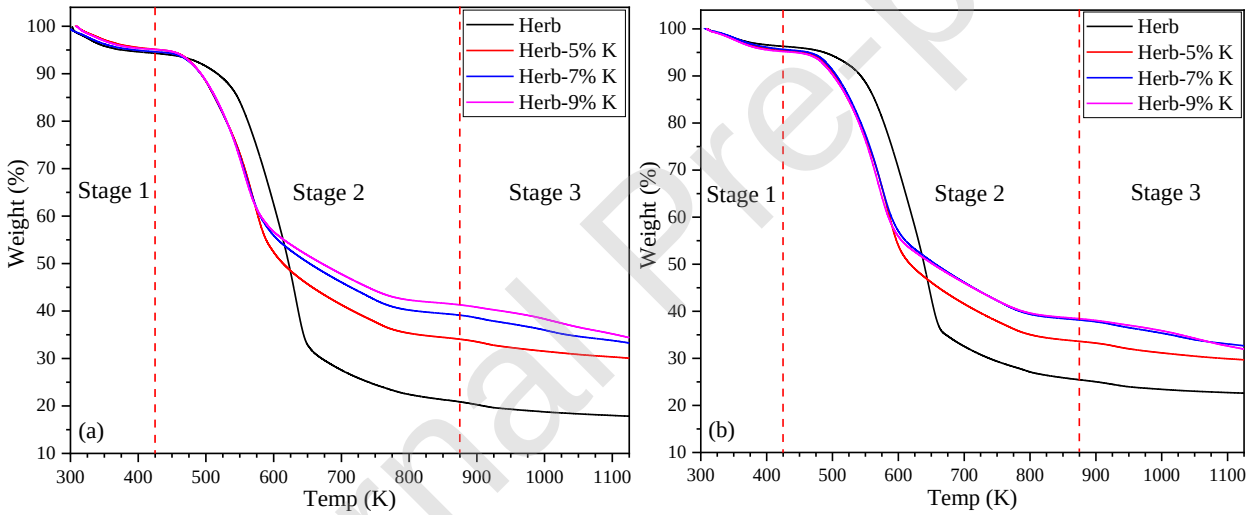

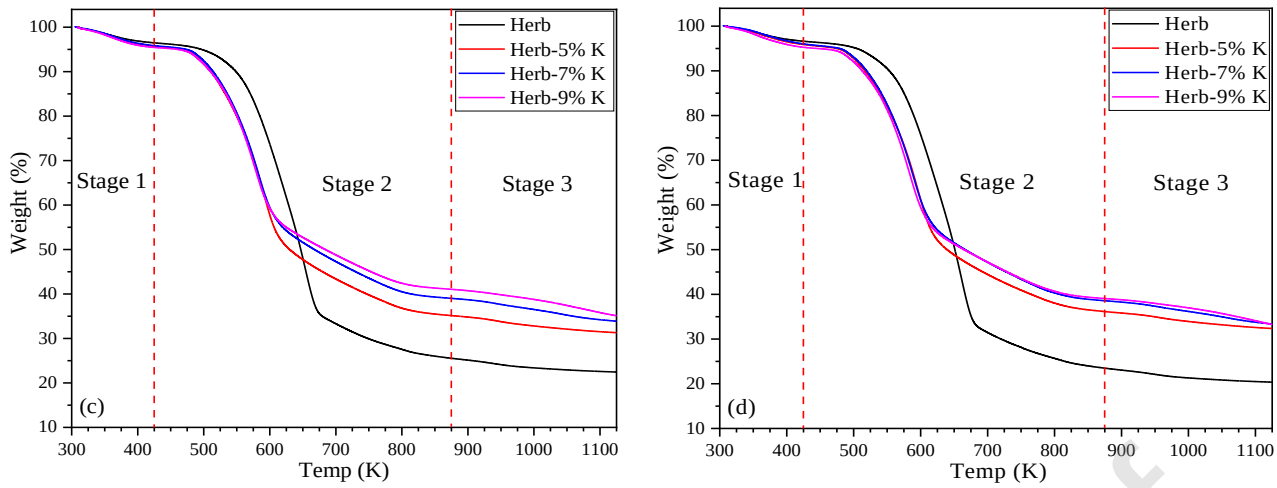

Figure 1: TG curves of herb samples with different K_2CO_3 loadings at (a)10 K/min (b)20 K/min (c) 30 K/min (d) 40 K/min.

Figure 1 shows the TG curves of CHR powders loading different proportions of K_2CO_3 catalyst at different heating rates of 10-40 K/min. At any of the four heating rates, the catalytic pyrolysis process of herb can be divided into three stages [5]: Stage 1-dehydration, Stage 2-devolatilization and Stage 3-carbonization. Table 4 lists the normalized mass loss of CHR for different samples: Δ $Mass_1$ (4.23 wt%- 7.94 wt%), Δ $Mass_2$ (82.02 wt%- 91.83 wt%) and Δ $Mass_3$ (3.68 wt%- 10.53 wt%) for three stages of the catalytic pyrolysis at different heating rates. The first stage is from 300K to 425K, which is mainly due to the removal of bound water and desorption of adsorbed gases and light volatiles, and it is usually called as dehydration. The second stage is from 425K to 875K, which is the major region for pyrolysis process as over 82.02% mass loss occurs, where most of the volatiles were decomposed and released. The last stage is carbonization at temperature above 875K, mainly dominated by the degradation of carbonaceous residues with little mass loss about 3.68%-10.53% [5].

Table 4: Normalized mass loss of CHR with different K_2CO_3 loadings determined by TGA.

Sample	Δ **$Mass_1$, %**					Δ **$Mass_2$, %**					Δ **$Mass_3$, %**				
	β_1	β_2	β_3	β_4	Mean	β_1	β_2	β_3	β_4	Mean	β_1	β_2	β_3	β_4	Mean
Herb	6.91	4.77	4.55	4.23	**5.12** ±1.22	89.41	91.57	91.47	91.83	**91.70** ±1.12	3.68	3.66	3.98	3.91	**3.81** ±0.16
Herb-5%K	6.96	6.50	6.21	6.05	**6.43** ±0.40	87.33	87.91	88.21	88.37	**87.97** ±0.46	5.45	5.60	5.61	5.58	**5.56** ±0.07
Herb-7%K	7.94	6.47	6.30	5.98	**6.67** ±0.87	83.28	85.36	85.93	86.21	**85.19** ±1.32	8.77	8.16	7.77	7.80	**8.13** ±0.46
Herb-9%K	7.45	7.08	7.02	7.07	**7.16** ±0.20	82.02	83.39	83.81	84.20	**83.36** ±0.95	10.53	9.53	9.17	8.74	**9.49** ±0.76

* The heating rates is β_1=10 K/min, β_2=20 K/min, β_3=30 K/min, β_4=40 K/min.

As a kind of special biomass waste, CHR mainly contains hemicelluloses, cellulose and lignin as well. Their DTG curves (Figure 2) show the typical pyrolysis characteristics of lignocellulosic biomass in the

devolatilization stage, which could be distinguished into two individual phases [19]: main devolatilization phase (425–700K for original herb sample, and 425-650K for catalytic samples) and continuous slight polycondensation phase (700–875 K for original herb sample, and 650-875K for catalytic samples), respectively. The normalized mass loss of CHR for this stage is determined by TGA data from 425-900K (Table S1). The first phase is a rapid weight-loss process, in which a large amount of volatile matter is released quickly. Generally, hemicelluloses and cellulose had high reactivity and could be completely decomposed in this phase [27], and the weight loss peaks of these two substances overlapped in DTG. For the second phase (>700 K), however, the TG curves decline slowly, and the DTG curves only show slight shoulder peaks with long tails. This is primarily due to the pyrolysis process of lignin with a relatively stable structure [28], and the slight polycondensation of the unstable bio-chars at a very slow pyrolysis rate [29]. Comparing the TG&DTG curves of CHR with different K_2CO_3 loadings, it is clear that K_2CO_3 catalysts made the TG&DTG curves move to the low temperature region comparing with the raw CHR sample, similar with the catalytic pyrolysis of cotton stalk [30] and sawdust [14].

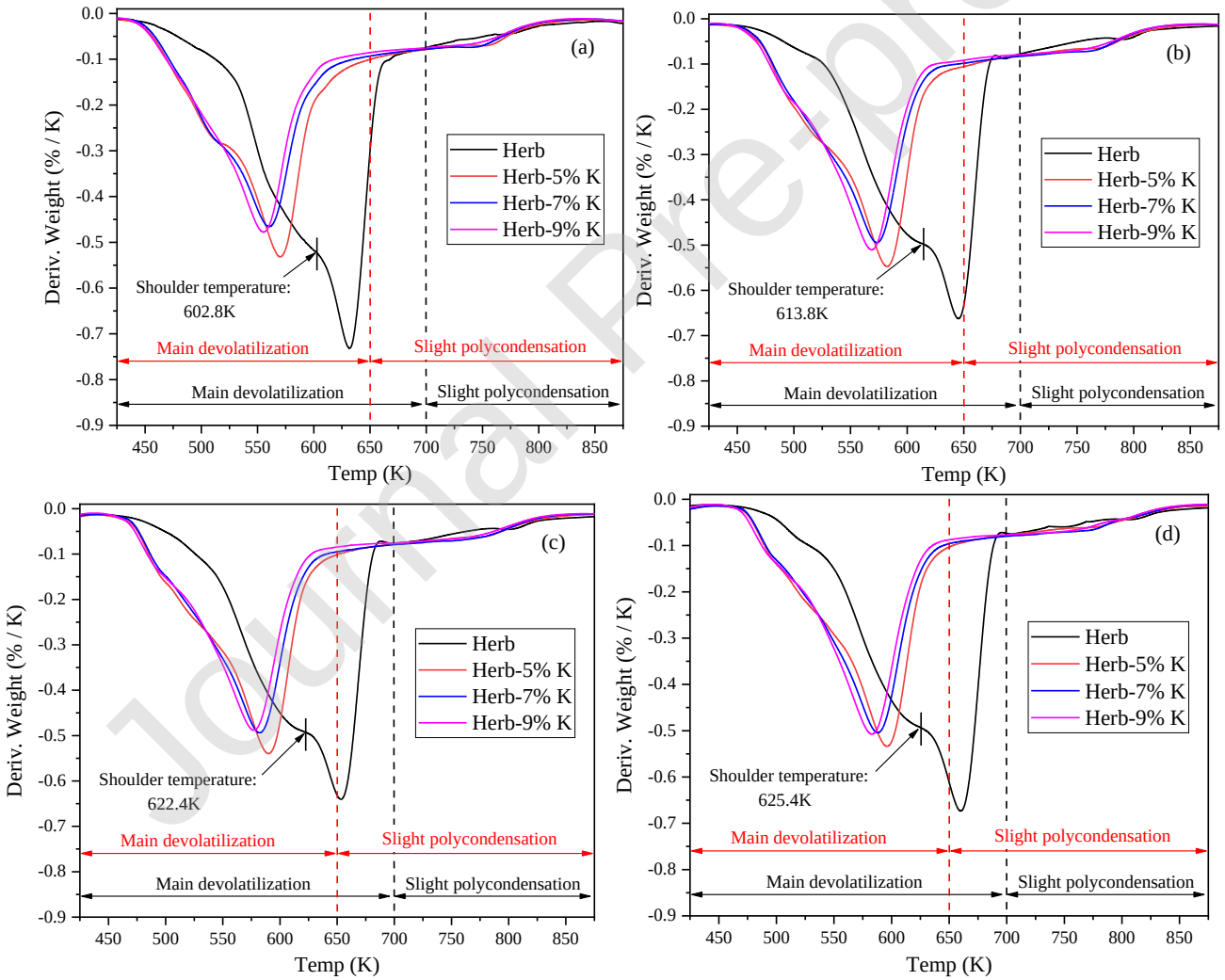

Figure 2: DTG curves of herb samples with different K_2CO_3 loadings at (a)10 K/min (b)20 K/min (c) 30 K/min

(d) 40 K/min.

The pyrolysis characteristic index D (%/K^4) is involved to evaluate the pyrolysis performance at the main devolatilization phase, which is defined as follows [5]:

$$D = \frac{\left(\frac{dw}{dt}\right)_{max}}{T_i \cdot T_{max} \cdot \Delta T_{1/2}} \tag{10}$$

Where $(dw/dt)_{max}$ (%/K) is the maximum rate of weight loss in the TG curve, T_{max} (K) is the temperature corresponding to the $(dw/dt)_{max}$, T_i (K) is the initial decomposition temperature, $\Delta T_{1/2}$ (K) is half-peak width, corresponding to the temperature range of the $(dw/dt)/(dw/dt)_{max}$=0.5.

T_{max} and D are two important characteristic parameters to evaluate the influence of K_2CO_3 loadings on pyrolysis performance of herb samples. As the heating rate increases from 10 K/min to 40 K/min, all the TG and DTG curves of different CHR samples slightly shift to the high temperature region as the increase of heating rate delays pyrolysis kinetics [31], this trend is reflected by T_{max} inconsiderably increasing with the increase of heating rate (shown in Figure 3). Meanwhile D slightly decreases with the increase of heating rate. Compared to the effect of heating up on characteristic parameters, the K_2CO_3 loading is the most significant influencing factor, T_{max} significantly decreases with the increase of K_2CO_3 loading (shown in Figure 3). Meanwhile D crucially increases with the increase of K_2CO_3 loading. It is easy to conclude that the effect of K_2CO_3 catalysts on the decomposition of CHR samples is most significant in the main devolatilization phase, which is the focus of this study.

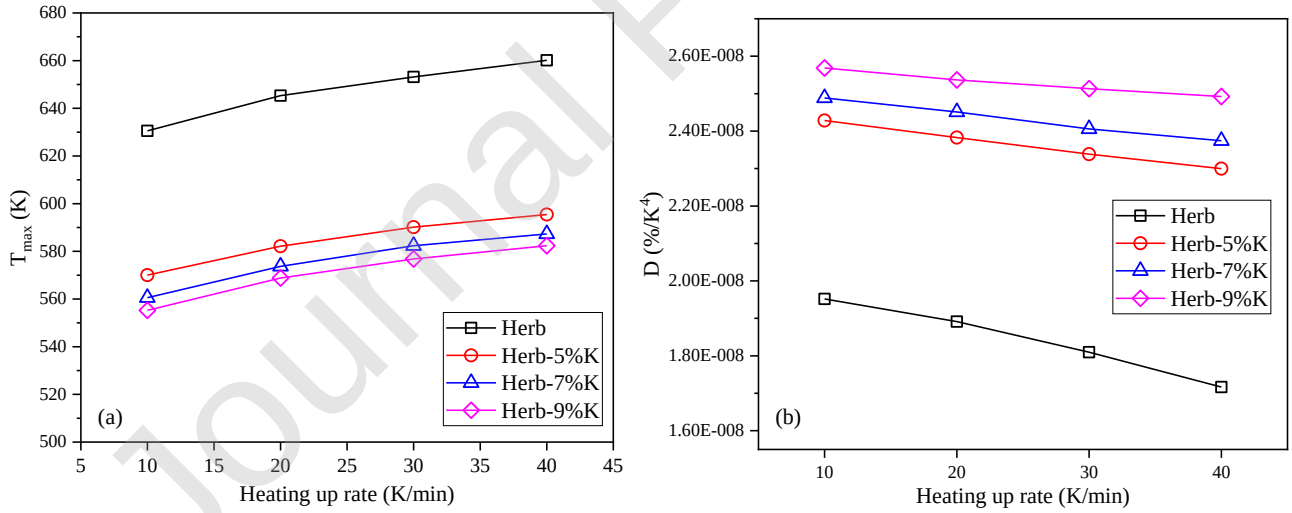

Figure 3: Characteristic parameters (a) T_{max} (b) D of herb samples with different K_2CO_3 loadings determined by TGA.

As shown in Figure 4, the DTG profiles of CHR samples have the typical curve shapes of lignocellulosic biomass pyrolysis: exhibited a steep decline with the presence of a maximum peak and a long tailing in the

devolatilization stage (425-875K). Interestingly, the DTG curve of raw CHR show an obvious shoulder peak and a maximum pyrolysis peak, owing to the pyrolysis behavior of hemicellulose overlapped with that of cellulose [6]. The DTG curve of CHR loading K_2CO_3 change into only one pyrolysis peak, which suggests that adding potassium salts promote CHR pyrolysis, leading to the coincidence of the main pyrolysis phase of cellulose and hemicellulose.

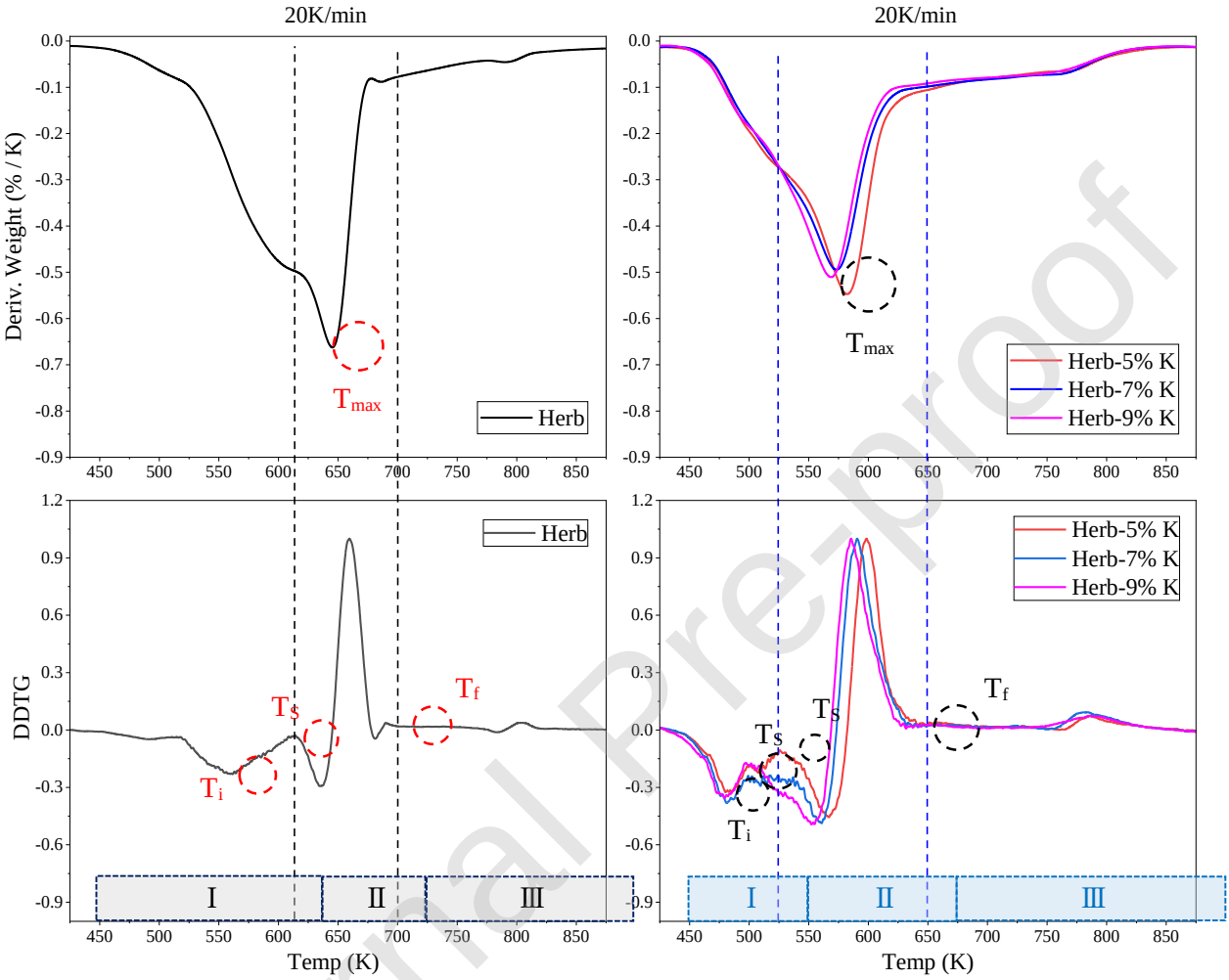

Figure 4: DTG profile and DDTG profiles of the devolatilization stage of CHR samples with different K_2CO_3 loadings at 20 K/min. (Section Ⅰ& Ⅱ belong to the main devolatilization phase)

Further analysis of the devolatilization stage is depicted by the second derivative of TG data (DDTG, Figure 4). Corresponding to the temperature points where $d^2m_t/m_0/dT^2$ is near to zero in DDTG profiles, the devolatilization stage could be further divided into three sub-sections: *Section Ⅰ* (425-615K for raw CHR, 425-525K for CHR with K_2CO_3), *Section Ⅱ* (615-700K for raw CHR, 525-650K for CHR with K_2CO_3) and *Section Ⅲ* (700-875K for raw CHR, 650-875K for CHR with K_2CO_3), corresponding to the thermal decomposition of the three pseudo components: hemicellulose, cellulose and lignin [6]. According to the temperature points in DDTG profiles corresponding to the local minima, one kind of shoulder peaks in DTG curves could be found

in *Section I* owing to the decomposition of hemicelluloses [6], and it is defined as T_s for the temperature corresponding to the shoulder peak. Another kind of sharp peaks in DTG curves appear in *Section II*, which attribute to the degradation of cellulose and partial depolymerization of lignin [6], and the temperature corresponding to the maximum DTG peak is defined as T_{max}. At high temperatures, the nearly horizontal straight lines appear in *Section III*, which attribute to the long tails with low weight loss rate in the DTG curves, relating to the slight polycondensation of aromatic rings in the complex structures of lignin [28].

As shown in Table 5, the effect of K_2CO_3 on catalytic pyrolysis of CHR is the most obvious in the main devolatilization phase (Section Ⅰ & Ⅱ, 425-700K). Due to the degradation of hemicellulose during decocting, T_s is about 615 K for the raw CHR, which is much higher than the pyrolysis temperature of hemicellulose of the traditional biomass (551K for the rape straw) [5]. On the other hand, the decoction process might change the three-dimensional structures of CHR materials, because the cellulose, hemicellulose and lignin could form a more complex network structure through chemical bonds like hydrogen bond and ether bond by hydrothermal treatment. As a result, both the T_{max} (645K) and T_f (700K) of the raw CHR are higher than those corresponding temperatures of (T_{max} = 605K, T_f = 650K) the rape straw. This also suggests that the energy consumption of CHR pyrolysis is much higher than the traditional biomass without decoction.

Table 5: The key temperature points for the main devolatilization phase at the heating rate of 20 K/min.

CHR Samples	T_S	T_{max}	T_i	T_f	$\Delta T_{1/2}$	ΔT_I	ΔT_{II}
Herb	614 K	645 K	561 K	700 K	97 K	190 K	85 K
Herb-5%K	525 K	582 K	483 K	650 K	82 K	100 K	125 K
Herb-7%K	500 K	573 K	482 K	650 K	75 K	75 K	150 K
Herb-9%K	500 K	568 K	479 K	650 K	74 K	75 K	150 K

* ΔT_I and ΔT_{II} represent the temperature interval of *Section I* and *Section II*, respectively; T_i and T_f are initial and finial decomposition temperature in the main devolatilization phase.

However, potassium salts could effectively promote the pyrolysis of the hemicellulose and cellulose for the CHR samples with K_2CO_3. Therefore, all of the key pyrolysis temperatures (T_i, T_{max} and T_f) in Table 5 decreased in sequence with the potassium loading of 5%, 7% and 9%. The lower T_i and T_S are, the easier the hemicellulose is thermally decomposed; meanwhile, the lower T_{max}, T_f and $\Delta T_{1/2}$ are, the earlier and more concentrated the peak of the volatile matter releasing occurs, mainly due to the degradation of cellulose. For CHR samples with K_2CO_3, therefore, the main pyrolysis phase of cellulose and hemicellulose significantly overlaps, the shoulder peaks are not distinct in the DTG curves owing to the hemicellulose decomposition, meanwhile ΔT_I narrows, and ΔT_{II} widens. Moreover, the catalytic effect of K_2CO_3 remains unchanged at the range of the potassium content >7%. In summary, the key pyrolysis temperatures decrease owing to the addition of K_2CO_3 catalyst favors the utilization of the CHR waste via pyrolysis and gasification, and 7%K content may be the suitable ratio for the potassium salt catalyst.

3.3 Kinetic analysis for the main devolatilization phase

3.3.1 Determination of activation energy

To accurately predict the catalytic pyrolysis characteristics in the main devolatilization phase, a model-free method of Starink is applied to analyze the kinetic parameters of CHRs loaded with different proportions of K_2CO_3. The specific calculation method of activation energy has been described in Section 2.3. The conversion rate (α) ranging from 0.1 to 0.8 with a step-size of 0.02 is adopted in this work. As shown in Figure 5, the curves for all samples have the similar trend: the $ln(\beta/T^{1.92})$ is linearly related with the $1/T$, and the slope of which is calculated to obtain the activation energy E_α. For α=0.1-0.8, the values of regression variance (R^2) are all exceed 0.99 (Table-S2), indicating that the activation energies are relatively accurate. K_2CO_3 catalyst significantly reduce the activation energy, and the pyrolysis characteristics of CHR samples are changed with the increase of the K concentration. However, satisfactory agreement is found on activation energies distribution between K-7% and K-9% samples, for their curves are almost overlapping with less than 2.74% deviation, which suggests that the suitable additive proportion of potassium should be about 7.0 % for the CHR material.

In particular, the values of R^2 and E_α become a little more volatile in higher conversions (α>0.70) for CHR samples with K_2CO_3. The small discrepancy should be caused by the combined effects of secondary reactions, diffusion and catalysis of potassium salts [32]. As is well known [33], the percentage variation between minimum and maximum activation energy should be less than 30%, when the one-step decomposition reaction could be used performing kinetic computations on thermal analysis data. Therefore, the conversion range of 0.10-0.74 is applied in next sections, where the apparent activation energies vary from 180 to 195 kJ/mol and 130 to 180 kJ/mol with a percentage of ~8.0% and ~20-30% for the raw CHR and the CHR with K_2CO_3. The average activation energy (E_0) of Herb, Herb-5%K, Herb-7%K and Herb-9%K are: 185.90 kJ/mol, 160.61 kJ/mol, 145.21 kJ/mol and 143.86 kJ/mol, respectively.

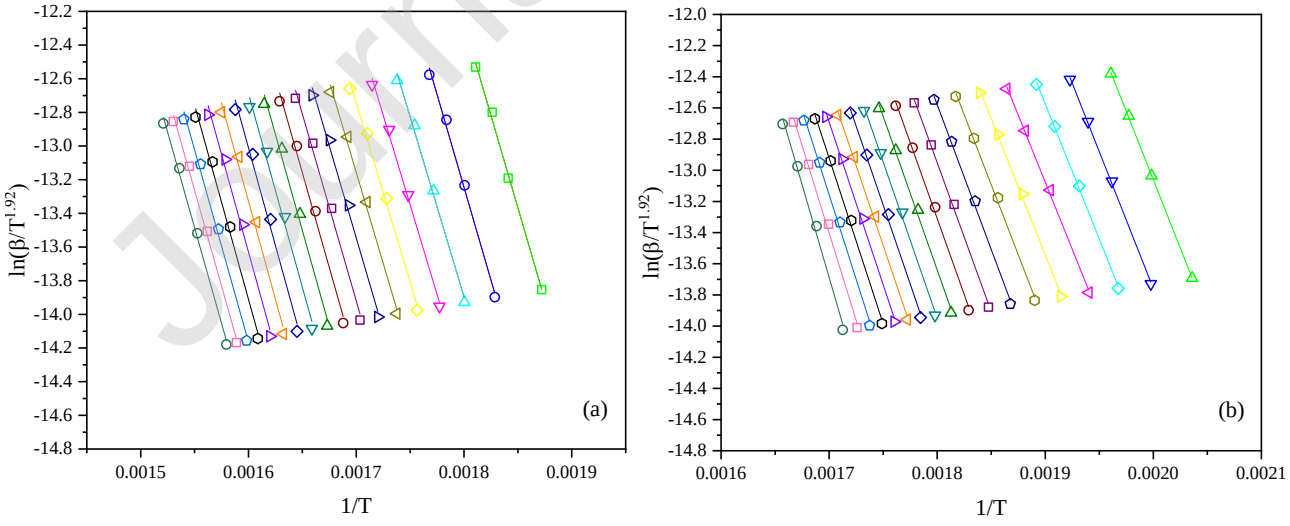

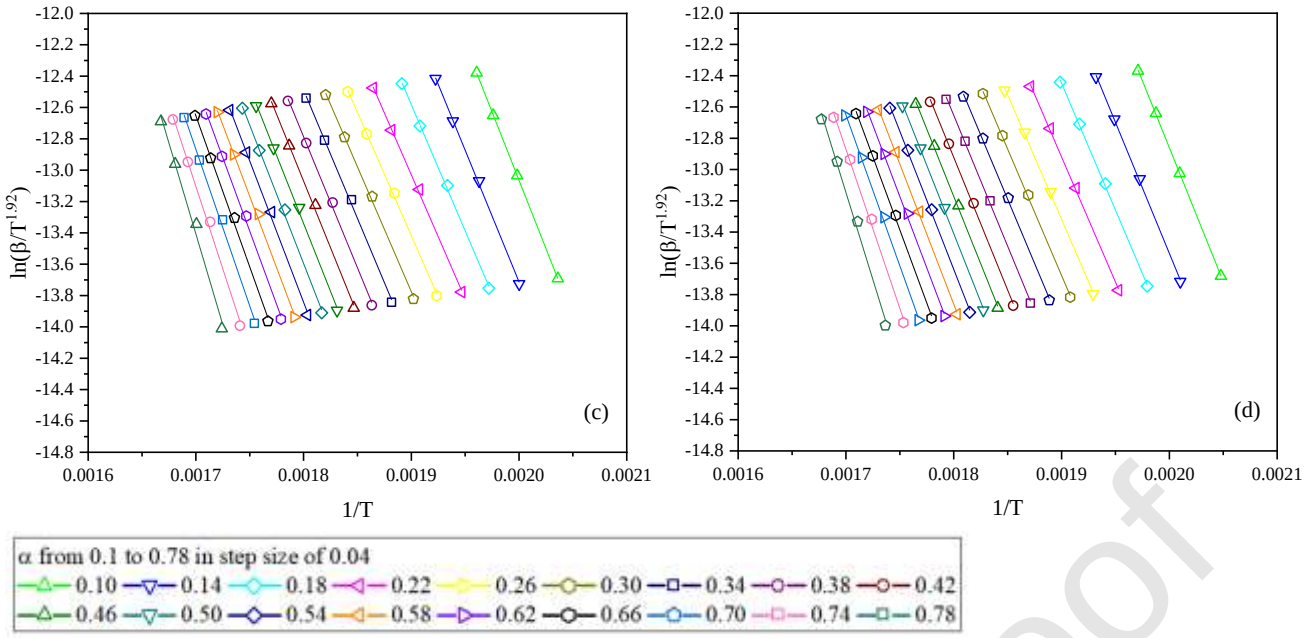

Figure 5: Kinetic plots of apparent activation energy as a function of conversion via Starink method. (a) Herb (b) Herb-5%K (c) Herb-7%K (d) Herb-9%K

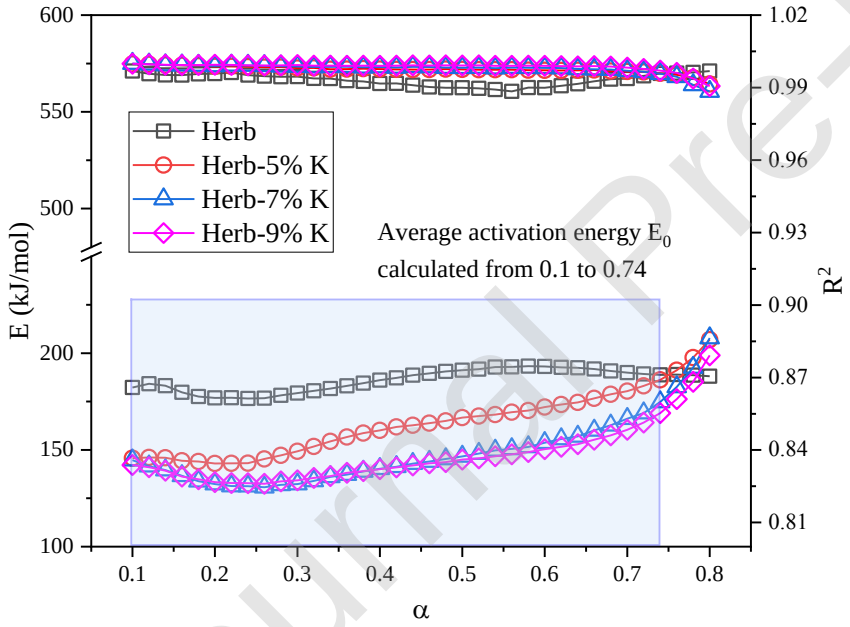

Figure 6: Variation of the thermal activation energy and the value of R^2. The calculated values are listed in Table S2.

3.3.2. Reaction model and pre-exponential factor

The E_0 obtained by Starink method is used to determine the reaction model and pre-exponential factor, since the method is found to be more efficient [23]. By plotting the theoretical (lines) and experimental (spots) master plots as a function of conversion rate in Figure 7, it is observed that experimental master plots give poor fits to

theoretical master plots based on the common reaction mechanisms ($G(\alpha)$, Table 3), even though experimental master plots at all heating rates are little close to the three-dimensional diffusion-Jander (D3) model when $\alpha<0.5$. As is noted by [33], D3-Jander equation (Eq. (14)) used the parabolic law (Eq. (11)) to define the thickness of the reaction zone (x, Eq. (12)) based on the assumption of spherical solid particles.

$$x^2 = kt \tag{11}$$

$$x = R\ (1-(1-\alpha)^{1/3}) \tag{12}$$

$$2\left(1-(1-\alpha)^{\frac{1}{3}}\right) = k't \tag{13}$$

Where k and k' are constant.

However, the parabolic law is the simplest rate equation for an infinite flat plane (one-dimensional (D1) model), where the conversion fraction (α) is directly proportional to product layer thickness (x). At present work, therefore, a modified D3-Jander model (D_n) is defined as Eq. (14), to describe the complex nonlinear relationship between α and x.

$$G(\alpha) = \left[1-(1-\alpha)^{\frac{1}{3}}\right]^n \tag{14}$$

Where n is the coefficient of the model. Substituting the Eq. (14) to Eq. (6), then, taking logarithm on both side of the equation, the following equation is given as:

$$\ln[P(u)] - \ln\left[\frac{\beta R}{E_\alpha}\right] = -\ln A + n\ln[1-(1-\alpha)^{1/3}] \tag{15}$$

The coefficient n of the D3 model and the pre-exponential factor A for different heating rates can be solved from Eq. (15) by plotting the linear fitting model of $\ln[P(u)] - \ln\left[\frac{\beta R}{E_\alpha}\right]$ against $\ln[1-(1-\alpha)^{1/3}]$, whose slope and intercept allow evaluation of the kinetic parameters n and A, respectively.

In Figure 7, The coefficients n of D_n model are depicted using the average values at different heating rates. The detailed results of the pre-exponential factor A and coefficient n are shown in Table 6.

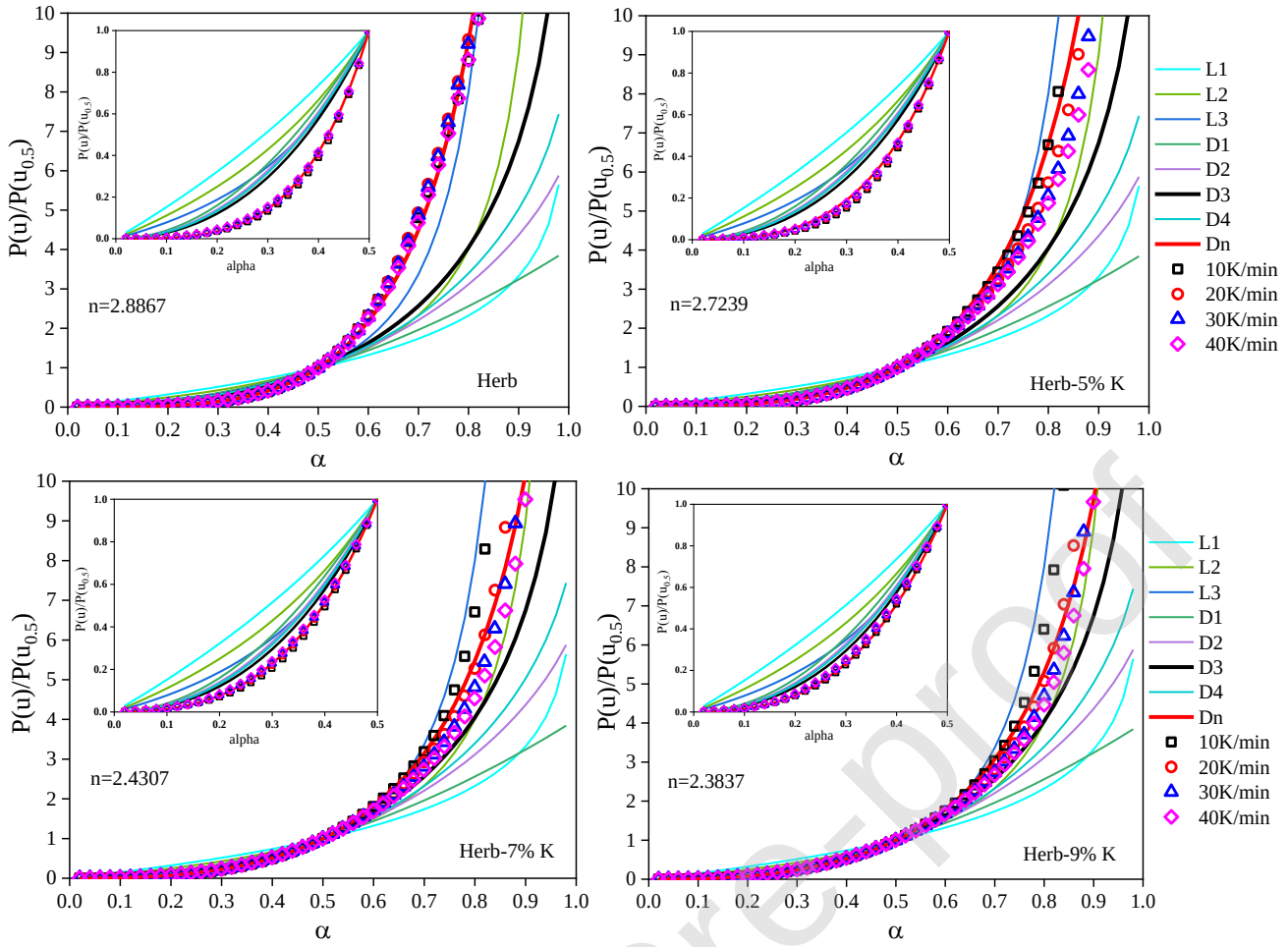

Figure 7: Experimental and theoretical master-plots of the CHR samples with different K_2CO_3.

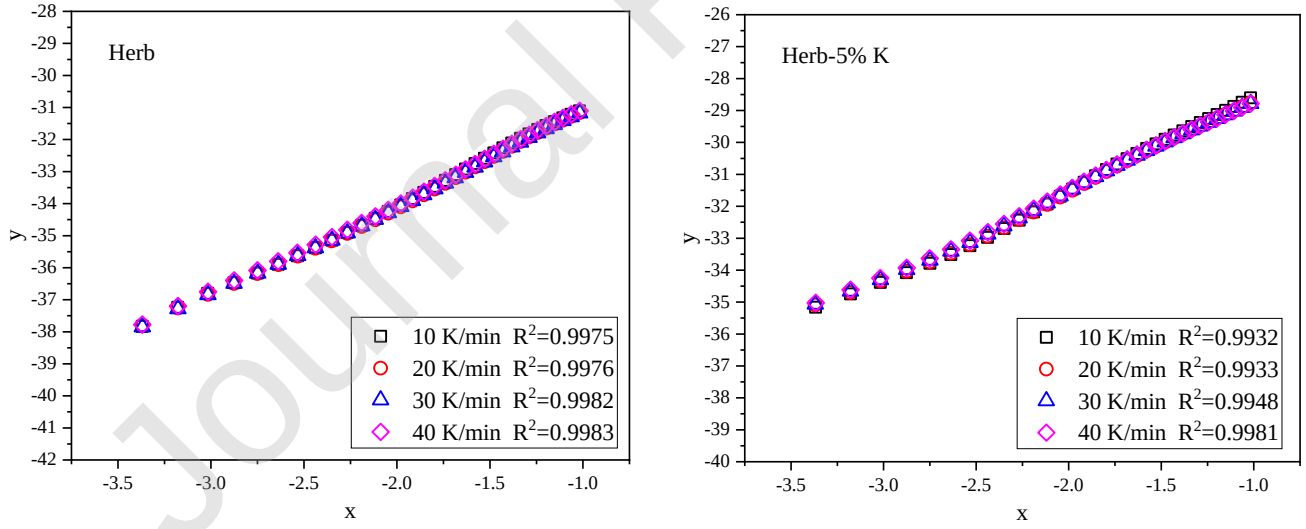

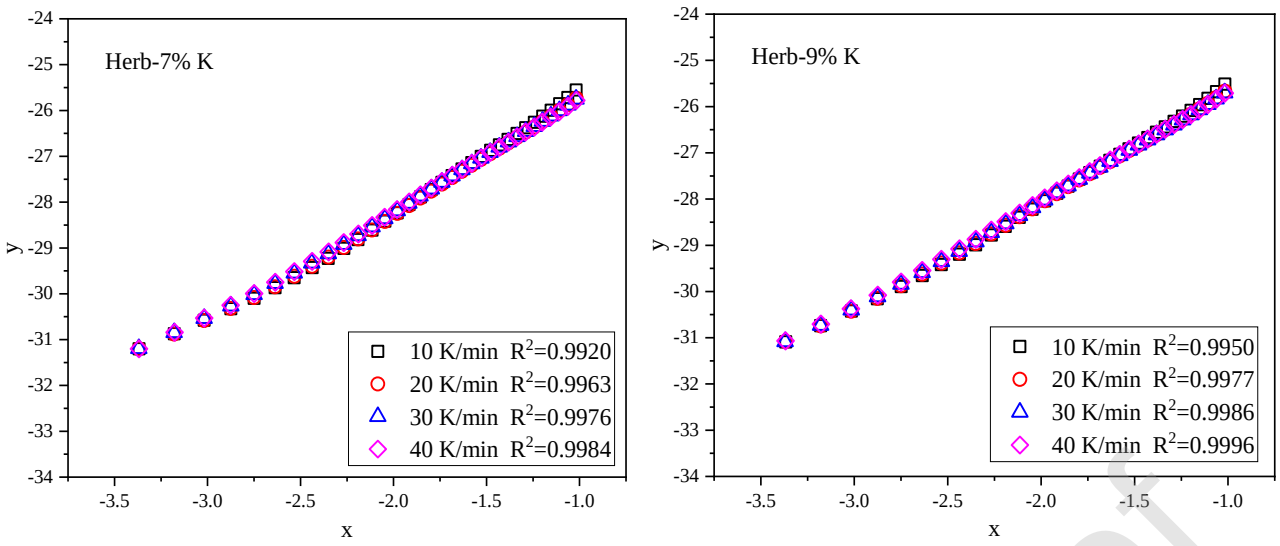

Figure 8: Linear fitting model of $y = \ln[P(u)] - \ln\left[\frac{\beta R}{E_\alpha}\right]$ against $x = \ln[1-(1-\alpha)^{1/3}]$. (Detailed parameters are listed in Table S4)

The experimental and D_n theoretical master plots of the raw CHR at different heating rates are almost overlap, while that of the CHR samples with K_2CO_3 have apparent differences after α>0.6 under different heating rates. The mechanism corresponds to D_n-Jander equation, indicating that reaction rate is mainly governed by diffusion for the main devolatilization stage of the raw CHR at all four heating rates. Therefore, the average values of *n* and *A* at the four heating rates can be used as the kinetic parameters for the raw CHR sample. However, for CHR samples with K_2CO_3, the experimental points become to discrete data at different heating rates as the temperature increase (α>0.5), and values of *n* and *A* tend to change measurably with the heating rates as shown in Figure 8. It possibly attributes to the significant catalytic effect of K_2CO_3 on the thermal decomposition of CHR samples at the higher temperatures. Consequently, for CHR with K_2CO_3, different values of *n* and *A* are selected at various heating rates, which is useful to improve the accuracy of kinetic parameters, as well as for the modeling of biomass catalytic pyrolysis.

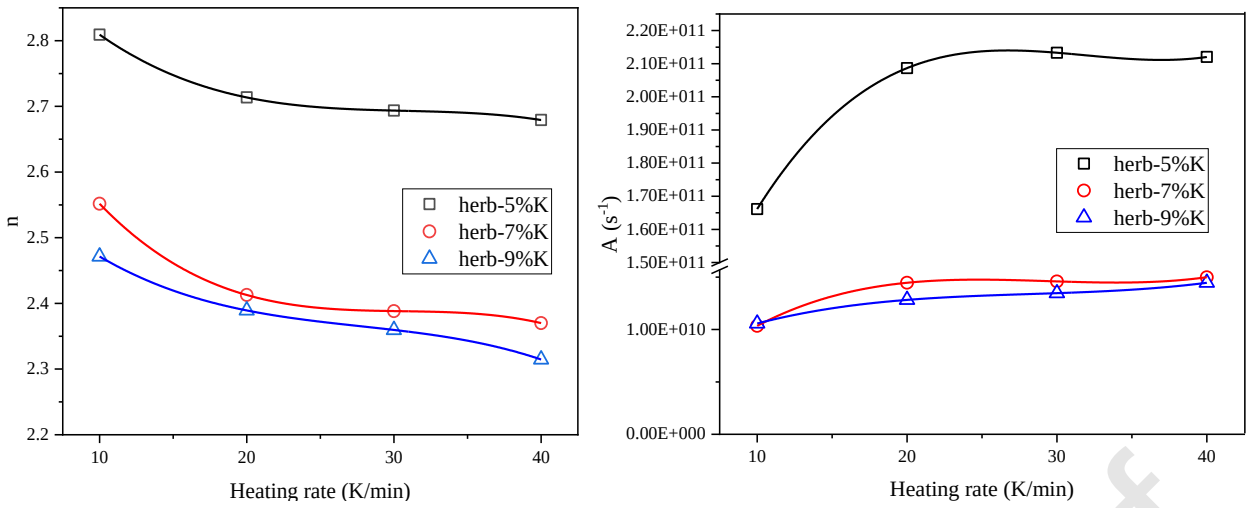

Figure 9: D_n coefficient and pre-exponential factor (the polynomials are listed in Table S3).

Table 6: The calculation results of herb samples (D_n coefficient and pre-exponential factor).

β	Herb		Herb-5% K		Herb-7% K		Herb-9% K	
	n	*A*/(s^{-1})	*n*	*A*/(s^{-1})	*n*	*A*/(s^{-1})	*n*	*A*/(s^{-1})
10K/min	2.9244	1.66×10^{12}	2.8092	1.66×10^{11}	2.5518	1.03×10^{10}	2.4714	1.06×10^{10}
20K/min	2.8766	1.94×10^{12}	2.7136	2.09×10^{11}	2.4128	1.45×10^{10}	2.3893	1.28×10^{10}
30K/min	2.8742	1.96×10^{12}	2.6936	2.13×10^{11}	2.3883	1.46×10^{10}	2.3596	1.35×10^{10}
40K/min	2.8717	1.79×10^{12}	2.6792	2.12×10^{11}	2.3700	1.50×10^{10}	2.3146	1.45×10^{10}
AVE	2.8867	1.84×10^{12}	2.7239	2.00×10^{11}	2.4307	1.36×10^{10}	2.3837	1.28×10^{10}

3.4 **Estimation of kinetic parameters by the D_n-Jader model**

CHR solid waste is a special kind of lignocellulosic biomass, which mainly consists of hemicellulose, cellulose and lignin as well. It had been reported that the activation energies of hemicellulose, cellulose and lignin were roughly in the range of 167-190 kJ/mol, 197-218 kJ/mol and 231-276 kJ/mol, respectively [34]. Thus, the average activation energies (E_0) obtained in this paper are in the reasonable ranges, though the E_0 of CHR loading catalysts is much lower than that of the raw CHR due to the catalysis of K_2CO_3. The values of E_0 (Table-S2), *A* and *n* with D_n-Jader model (Table-S4) were employed to elaborate the kinetic parameters of the CHR pyrolysis in the main devolatilization stage.

With respect to TG curves (Figure 10), good fitting qualities are observed with R^2>0.995 for the raw CHR at all the four heating rates. For the CHR samples with K_2CO_3, however, R^2 values at lower heating rates (β≤20K) are a little bit below 0.995, especially in the high temperatures (>575K). This is still a good agreement; the small

deviation might be caused by the combined effects of secondary reactions due to the K_2CO_3 catalysis of biomass char and lignin under high temperatures [34], which indicates that the catalytic pyrolysis reactions should require complex multi-step kinetic pathways, and could not be perfectly described by the simple parameters of single-step kinetics.

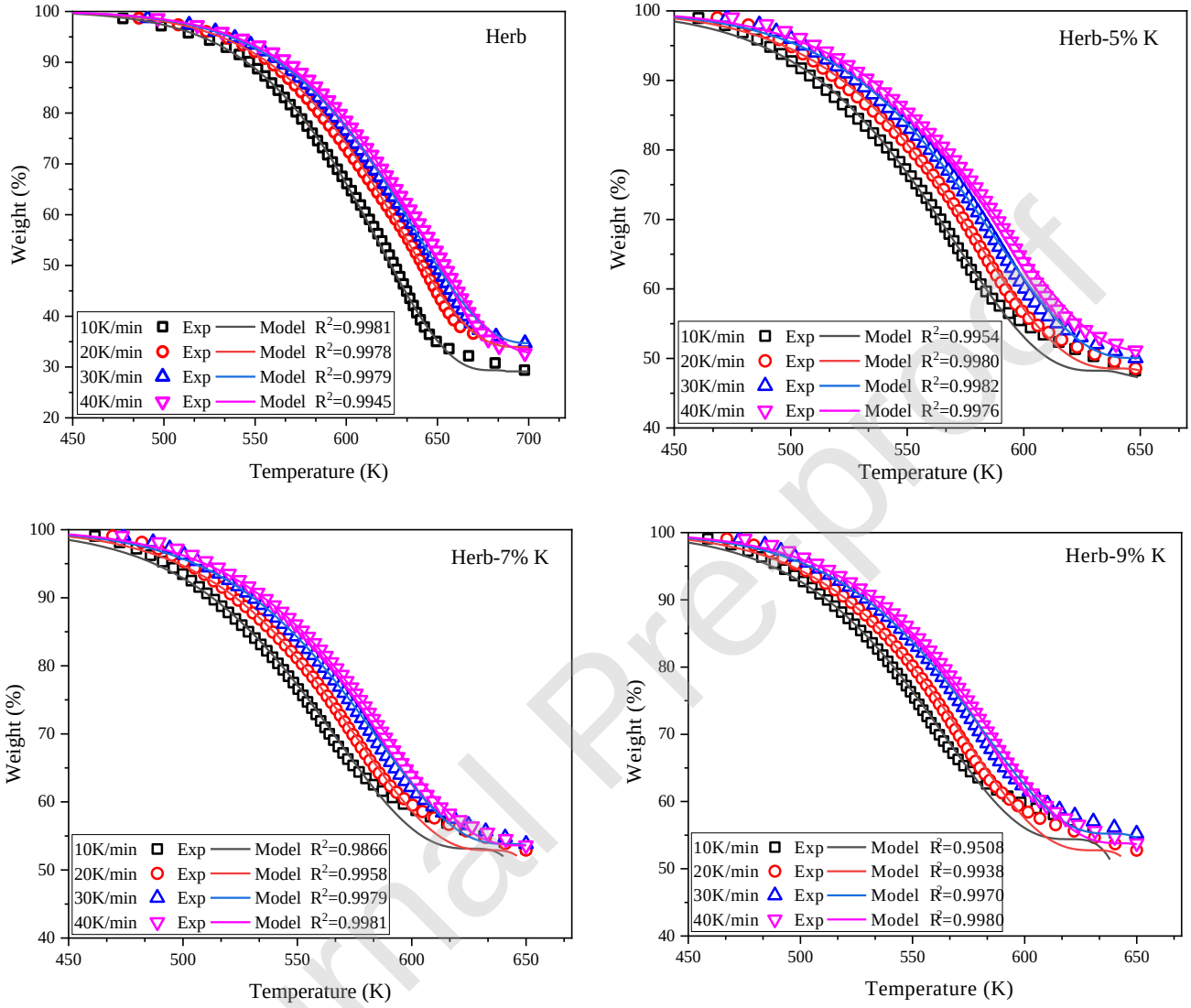

Figure 10: Calculated TG curves based on the D_n-Jader model compared with experimental data at various heating rates.

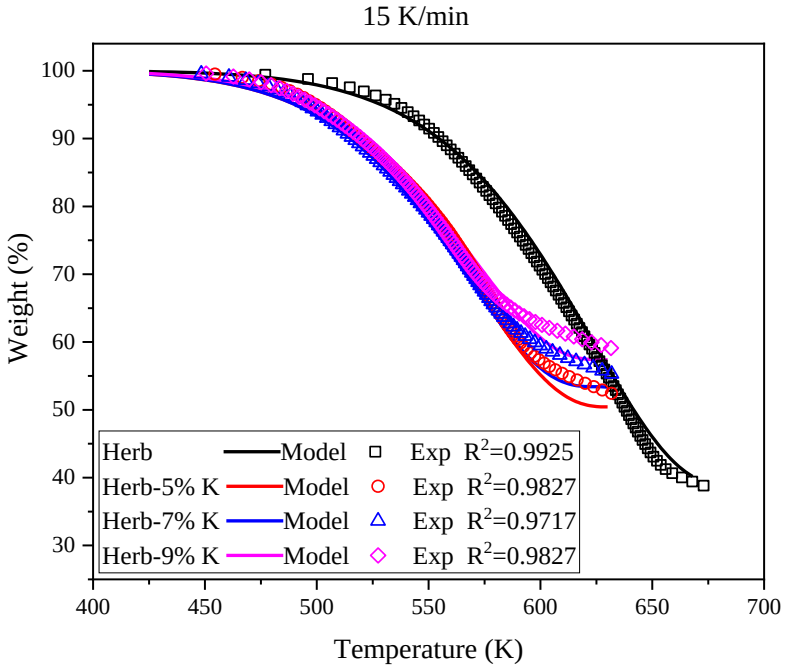

Figure 11: Comparison between TG data and fitted curves for different samples at 15K/min.

In addition, in order to evaluate the predictive ability and applicability of the model parameters, β_1, β_2, β_3 and β_4 profiles are adopted to calculate the kinetic parameters by Starink method, and predicted model results for the β_5 (15K/min) cases based on the optimized parameters are plotted in Figure 11. From Figure 9, we can use 3rd order polynomials to express the relationship between the heating rate (β) and the pre-exponential factor (A), and the relationship between the heating rate (β) and the coefficient n. Then, the TG data of the herb samples with different K_2CO_3 concentration could be obtained at the heating rate of 15 K/min. The fitted curves of coefficient n and A are listed in Table S3. Figure 11 shows the comparison between experimental TGA data and the fitted curves of different samples at 15 K/min. The predicted results are in very good agreement with experimental data with R^2=0.9925 for the raw CHR, and R^2>0.97 for the CHR with K_2CO_3, which means that the D_n-Jader model parameters can be applied not only to conditions where they are obtained, but also to conditions beyond. The differences between model and experimental data above 575K is owing to the increased activation energy for the CHR with K_2CO_3, which is not appropriately interpreted by averaged activation energy (E_0) used in the model. In sum, the optimized parameters in this work would provide the basis data for forecasting the pyrolysis properties and designing the pyrolyzer for the CHR solid waste in real conditions with various heating rates.

4. **Conclusion**

The catalytic pyrolysis of CHR solid waste loading K_2CO_3 was studied by the non-isothermal temperature-

programmed thermogravimetry. The pyrolysis temperature of the raw CHR is higher than traditional lignocellulosic biomass without decoction. K_2CO_3 catalysts significantly promote the catalytic pyrolysis reaction of the hemicellulose and cellulose of CHR samples at the main devolatilization stage from 425K to 700K, which is the major pyrolysis region as over 80.0% mass loss occurs. The pyrolysis kinetics were found to be successfully described by using the model-free Starink method. The estimated average activation energy (E_0) of Herb, Herb-5%K, Herb-7%K and Herb-9%K are: 185.9kJ/mol, 160.6kJ/mol, 145.2kJ/mol and 143.8 kJ/mol, respectively. By using the generalized master-plots method, it was found that the CHR pyrolysis was governed by a modified D_n-Jader model $G(\alpha) = \left[1-(1-\alpha)^{\frac{1}{3}}\right]^n$, but values of n and A tend to change measurably with heating rates for the CHR samples with catalysts due to the remarkably catalytic effect of K_2CO_3. The model results using the optimized parameters were highly consistent with experimental TG data at all the four heating rates for the raw CHR, however, there is small discrepancy for that of the CHR samples with K_2CO_3, caused by the presence of multi-step complex decomposition reactions at high temperatures. Besides, cross-validation showed that the kinetic parameters can be applied not only to heating rates where they were obtained, but also to the other heating rate; which indicates that the current work provides a simple route for the kinetic analysis of catalytic pyrolysis of CHR solid waste, especially in the real scenarios with various and mutative heating rates.

Authors statement

Hongyu Zhu: Methodology, Software, writing, visualization, Formal analysis.

Lin Lang: Conceptualization, Methodology, Validation, visualization, Formal analysis, Writing - Review & Editing

Gang Fang: Methodology, TG experiments, Data Curation

Dingying Na: TG experiments, Data Curation

Xiuli Yin: Supervision, Funding acquisition,

Xi Yu: Conceptualization, Methodology, Software, visualization, Formal analysis, Writing - Review & Editing

Chuangzhi Wu: Supervision, Funding acquisition

Anthony V. Bridgwater: Supervision, Funding acquisition

Conflicts of Interest Statement

The authors whose names are listed immediately below certify that they have NO affiliations with or involvement

in any organization or entity with any financial interest (such as honoraria; educational grants; participation in speakers' bureaus; membership, employment, consultancies, stock ownership, or other equity interest; and expert testimony or patent-licensingarrangements), or non-financial interest (such as personal or professional relationships, affiliations, knowledge or beliefs) in the subject matter or materials discussed in this manuscript.

Acknowledgments

The authors gratefully acknowledge the financial support from the National Key R&D Program of China (2019YFB1503905), the National Natural Science Foundation of China (51676192), and the Guangdong International Science and Technology Innovation Fund (2019A050510031). Hongyu Zhu gratefully acknowledges Doctoral Training Programme fund from College of Engineering and Physical Sciences, Aston University.

References

[1] F. Guo, Y. Dong, T. Zhang, L. Dong, C. Guo and Z. Rao, *Industrial & Engineering Chemistry Research*, 53, (2014) 13264.
[2] Y. Li, J. Wang, Y. Liu, X. Luo, W. Lei and L. Xie, *Journal of General Virology*, 101, (2020) 1079.
[3] T.T. Li, F.Q. Guo, X.L. Li, Y. Liu, K.Y. Peng, X.C. Jiang and C.L. Guo, *Waste Management*, 76, (2018) 544.
[4] P. Wang, S.H. Zhan, H.B. Yu, X.F. Xue and N. Hong, *Bioresource Technology*, 101, (2010) 3236.
[5] L. Xu, Y. Jiang and L. Wang, *Energy Conversion and Management*, 146, (2017) 124.
[6] T.P. Wang, L. Peng, Y.N. Ai, R.H. Zhang and Q. Lu, *Journal of Analytical and Applied Pyrolysis*, 129, (2018) 61.
[7] A.Z. Xu, W.H. Zhou, X.D. Zhang, B.F. Zhao, L. Chen, L.Z. Sun, W.J. Ding, S.X. Yang, H.B. Guan and B. Bai, *Journal of Analytical and Applied Pyrolysis*, 130, (2018) 216.
[8] B.F. Zhao, G. Song, W.H. Zhou, L. Chen, L.Z. Sun, S.X. Yang, H.B. Guan, D. Zhu, G.Y. Chen, W.J. Ding, J.W. Wang and H.J. Yang, *Energy & Fuels*, 34, (2020) 1131.
[9] J.H. Park, Y.K. Park and Y.M. Kim, *Environmental Research*, 187, (2020).
[10] B. Zhang and J. Zhang, *Energy & Fuels*, 31, (2017) 9627.
[11] W.J. Ding, X.D. Zhang, B.F. Zhao, W.H. Zhou, A.Z. Xu, L. Chen, L.Z. Sun, S.X. Yang, H.B. Guan, X.P. Xie, G.Y. Chen, L. Zhu and G. Song, *Journal of Analytical and Applied Pyrolysis*, 134, (2018) 389.
[12] B.F. Zhao, X.D. Zhang, A.Z. Xu, W.J. Ding, L.Z. Sun, L. Chen, H.B. Guan, S.X. Yang and W.H. Zhou, *Science of the Total Environment*, 626, (2018) 703.
[13] R.H. Venderbosch, *ChemSusChem*, 8, (2015) 1306.
[14] W.H. Zhou, B. Bai, G.Y. Chen, L.L. Ma, D.W. Jing and B.B. Yan, *International Journal of Hydrogen Energy*, 43, (2018) 13829.
[15] Q.-V. Bach and W.-H. Chen, *Bioresource Technology*, 246, (2017) 88.
[16] R.K. Mishra and K. Mohanty, *Bioresource Technology*, 251, (2018) 63.
[17] M.J. Starink, *Thermochimica Acta*, 404, (2003) 163.
[18] A. Khawam and D.R. Flanagan, *Journal of Physical Chemistry B*, 110, (2006) 17315.
[19] Y.S. Lin, H.M. Xiao, B.M. Chen, Y. Ge, Q. He, S. Tao and W.H. Wang, *Bioresource Technology*, 304, (2020).
[20] Y. Lin, Y. Tian, Y. Xia, S. Fang, Y. Liao, Z. Yu and X. Ma, *Bioresource Technology*, 273, (2019) 545.
[21] M. Radojević, B. Janković, V. Jovanović, D. Stojiljković and N. Manić, *PLOS ONE*, 13,

(2018) e0206657.

[22] S. Vyazovkin, A.K. Burnham, J.M. Criado, L.A. Pérez-Maqueda, C. Popescu and N. Sbirrazzuoli, *Thermochimica Acta*, 520, (2011) 1.

[23] M.J. Starink, *Thermochimica Acta*, 288, (1996) 97.

[24] N. Koga and J.M. Criado, *Journal of the American Ceramic Society*, 81, (1998) 2901.

[25] F.J. Gotor, J.M. Criado, J. Malek and N. Koga, *The Journal of Physical Chemistry A*, 104, (2000) 10777.

[26] W.-H. Chen, B.-J. Lin, M.-Y. Huang and J.-S. Chang, *Bioresource Technology*, 184, (2015) 314.

[27] M. Nishimura, S. Iwasaki and M. Horio, *Journal of the Taiwan Institute of Chemical Engineers*, 40, (2009) 630.

[28] Z. Luo, S. Wang and X. Guo, *Journal of Analytical and Applied Pyrolysis*, 95, (2012) 112.

[29] J. Wannapeera and N. Worasuwannarak, *Journal of Analytical and Applied Pyrolysis*, 115, (2015) 279.

[30] M.Q. Chen, X.Y. Qi, J. Wang, M.G. Chen, F. Min, S. Liu and B. Jing, *Ranliao Huaxue Xuebao/Journal of Fuel Chemistry and Technology*, 39, (2011) 585.

[31] J.-L. Shie, C.-Y. Chang, J.-P. Lin, C.-H. Wu and D.-J. Lee, *Journal of Chemical Technology & Biotechnology*, 75, (2000) 443.

[32] A. Anca-Couce, A. Berger and N. Zobel, *Fuel*, 123, (2014) 230.

[33] S. Vyazovkin, A.K. Burnham, J.M. Criado, L.A. Perez-Maqueda, C. Popescu and N. Sbirrazzuoli, *Thermochimica Acta*, 520, (2011) 1.

[34] J. Cai, W. Wu, R. Liu and G.W. Huber, *Green Chemistry*, 15, (2013) 1331.